Appendix H

Calibrations tests

In this chapter we enumerate the experiments we performed in order to test the performance and accuracy of the Minibird tracker. The experiments had two goals:

- test in depth the communication and data formats of the device.
- build the software able to model the calibration.
- estimate the real accuracy of the tracker, and its drawbacks for real applications.

We recall the equation which gives final the coordinates $C_{\overline{\mathbf{x}}}$ as a function of the pixel coordinates $P_{\overline{\mathbf{x}}}$, and other transformation matrices:

$$C_{\overline{\mathbf{x}}} = P_{\overline{\mathbf{x}}} \cdot M_U^R \cdot M_R^T \cdot M_T^C \tag{H.1}$$

In all these experiments, $P_{\overline{\mathbf{x}}} = (0, 0)$, but we leave this term in order to keep the same notation we employed for the ultrasound calibration. M_R^T, the receiver to transmitter matrix, is output by the tracker and gives the position and orientation at each moment. Now our goal is to combine the other terms of the equations, $C_{\overline{\mathbf{x}}}$ and M_T^C in order to produce a system with more equations than unknowns which permits to find the unknown term M_U^R.

But now the tracker is not attached to the ecographer. Instead, two configurations are tested; in the first, the receiver is hand-held freely and thus M_U^R is taken as the identity matrix. For this case, we are interested only in determining the values of M_T^C and estimate the resulting accuracy. In the second configuration the receiver is rigidly attached to a stylus, and M_U^R actually depends only on the coordinates of the tip of the stylus in the receiver coordinate system.

One possible way to calibrate the system is to restrict the movement of the object (receiver or stylus) to some know geometrical figure, which could be a plane, line or point. Then, the final coordinates of the object, $C_{\overline{\mathbf{x}}}$, would hold a geometric property enabling to set a system of equations. For instance, if we restrict the movement of the stylus to a single point by attaching the tip to a small hole and moving the rest freely, we can constraint the coordinates of the stylus in the cuberille coordinates to a constant, e.g.,

$$C_{\overline{\mathbf{x}}} = (x', y', z') = (0, 0, 0) \tag{H.2}$$

This equation gives a system of three equations per position recorded by the tracker. Similarly, constraining the movement of the tip to a plane (the flat surface of a table, for instance) would give a single equation per position, $z' = 0$.

The system of equations must then be processed using some numerical algorithm in order to find the unknown variables. In the appendix G we have already described the relevant mathematical issues.

Following we list the experiments done; the label will be used for reference in the text from now on.

RP1 Receiver on plane.

RP2 Receiver on plane, pausing to capture values.

RP3 Receiver attached to a heavy object, moving freely on a plane.

RL Receiver moving on a line.

SP Stylus moving on a plane.

SL Stylus following a linear trajectory.

SS Stylus restricted to a spot.

Each configuration determines a different set of identifiable parameters:

	Parameters	Receiver only		Stylus		
		Plane	line	Plane	Line	Point
		RP1–4	*RL*	*SP*	*SL*	*SS*
M_U^R	T_x	–	–	Y	Y	Y
	T_y	–	–	Y	Y	Y
	T_z	–	–	Y	Y	Y
M_T^C	T_x	–	–	–	–	Y
	T_y	–	Y	–	Y	Y
	T_z	Y	Y	Y	Y	Y
	R_x	Y	–	Y	–	–
	R_y	Y	Y	Y	Y	–
	R_z	–	Y	–	Y	–

Table H.1: Identifiable parameters for each model

H.1 RP1

The first experiment consisted on estimating the coordinates of a flat surface in the tracking coordinates system. In addition to the accuracy, we were interested in seeing how reproducible were the results. For this purpose, we took five sets of values in two different positions. In this configuration, the transmitter was placed slightly below the surface. For the second set, the transmitter orientation was changed. The sixth set of values was the union of the previous sets of values.

For this configuration, as for **RP2–4**, the matrix M_U^R has been taken as identity. We measure the accuracy with the root mean squared value between the expected and the real position (see appendix G). The condition number is an indication of how well defined the system is. Mathematically, it is the ratio between the highest and the lowest variation in the magnitude of parameters (again see the mentioned appendix). It is accepted that well posed systems have a condition number lower than 100.

In the mathematical system the condition number can be expected to be high, since the magnitudes of the variables are very different; see, in table H.1, that while T_z, the translation, raises up to 90, the rotation variables are very low. There is a mathematical solution to this problem, which is to scale the variables until all have a similar magnitude. The alternative set of equations will have lower condition number, and the optimisation algorithm is expected to present better convergence properties. Therefore, the solutions for one set and the other are often not the same. For this experiment and for **RP2–4**, however, both sets converged to the same solution.

S.	#	T_z (mm)	R_x (deg)	R_y (deg)	RMS (mm)	StdDev (mm)	C.N.	C.N. Scaled
1	323	88.29	0.42	1.26	0.53	0.66	967.68	7.53
2	340	88.89	0.26	1.09	0.59	0.73	1066.7	8.07
3	334	88.06	0.15	1.2	0.77	0.97	1100.64	8.84
4	323	89.35	0.43	1.17	0.93	1.22	965.63	7.69
5	338	89.88	0.17	0.93	0.89	1.06	837.14	6.76
6	1658	89.	0.26	1.08	0.85	1.1	953.29	7.49
1	313	81.06	13.81	-1.08	0.56	0.68	1505.27	12.08
2	309	79.91	13.53	-1.07	0.67	0.88	1331.76	10.42
3	353	78.91	13.62	-0.88	0.6	0.88	1449.82	10.67
4	316	80.52	13.65	-1.19	0.43	0.59	1302.64	10.23
5	313	80.02	13.53	-1.09	0.43	0.53	1185.79	9.75
6	1604	80.19	13.62	-1.1	0.57	0.8	1318.63	10.32

Table H.2: Numerical results for experiment **RP1**. S, set; #, number of collected points.

Results in table H.1 show an error lower than $1mm$, and also the condition number is good, lower than 100. To further investigate the nature of the error, we present in the next page several graphical functions. See that the error changes smoothly per frame.

However, the solutions present relatively high variations for the parameter T_z. This probably is an indication that the data set is not as well posed as one would desire, i.e., the profile of the error is low not at a single point but rather in a wider area. To investigate this hypothesis, we have computed the error for values varying from solution 1 to 5 of the first dataset, using the full data as input values. In bottom right graphic in H.1, the rms error at $x = 0$ is computed for solution 1, $x = 10$ at solution 2, etc., while intermediate values are computed at linear values between the other solutions.

The resulting graphic demonstrates that the function has a valley-like shape at the minimum, and that the optimisation algorithm may converge at any point in it.

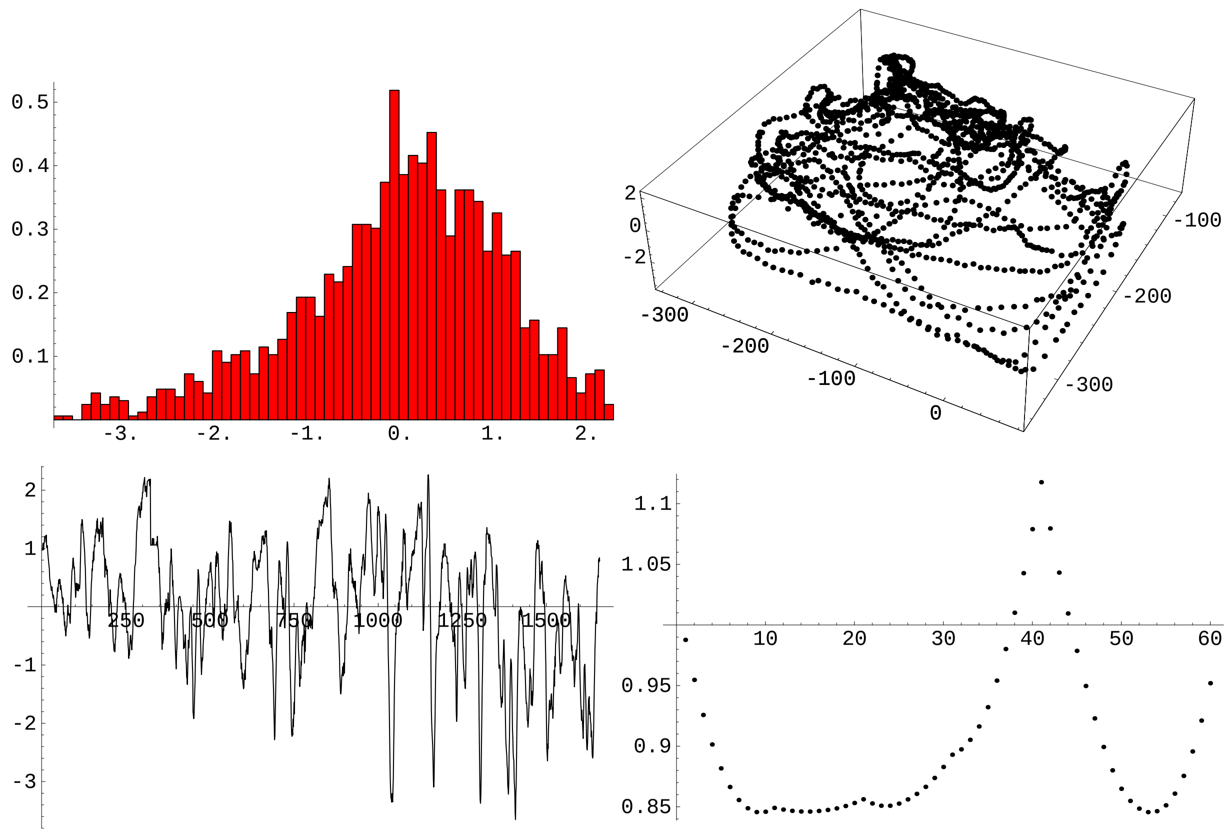

Figure H.1: Graphical results for experiment **RP1**.Top left: the histogram of errors. Top right: the error as the z position for each (x, y) position. Bottom left: error per frame. Bottom right: errors for each set of solutions. Units in mm.

H.2 RP2 and RP3

In this experiment we wanted to see the influence of the movement of the receiver for the final accuracy. The motivation was that when we moved the receiver in a rapid fashion and then stop it suddenly, the coordinates took some time before becoming stable. Thus we made the hypothesis that the tracker gave worse accuracy when in motion.

The settings of the experiments are the same as in the previous: two different configurations, and five data sets for each.

S.	#	T_z (mm)	R_x (deg)	R_y (deg)	RMS (mm)	StdDev (mm)	C.N.	C.N. Scaled
1	22	87.1	-179.72	-1.55	0.19	0.29	1017.08	10.67
2	18	87.58	0.09	1.44	0.31	0.39	855.89	8.11
3	18	86.98	0.21	1.6	0.2	0.25	975.74	9.38
4	20	87.69	0.28	1.53	0.3	0.38	1068.47	10.04
5	15	88.16	0.46	1.52	0.22	0.33	1040.41	10.22
6	93	87.26	0.2	1.54	0.33	0.43	930.8	9.02
1	18	78.9	13.46	-0.98	0.23	0.28	1584.76	15.05
2	18	79.45	13.7	-1.03	0.17	0.24	1777.64	15.02
3	18	78.85	13.44	-0.99	0.24	0.32	1500.59	12.79
4	20	80.16	13.69	-1.14	0.17	0.22	1394.64	12.04
5	20	80.06	13.66	-1.18	0.2	0.28	1347.09	11.44
6	94	79.64	13.62	-1.09	0.24	0.31	1407.56	12.17
RP3	494	116.28	13.57	-0.69	0.22	0.29	2887.58	20.7

Table H.3: Numerical results for experiment **RP2**

The results confirmed this hypothesis: the rms is clearer lower than the previous experiment.

We designed a very similar experiment to test graphically the sensitivity to the movement: we attached the sensor to a heavy object, which could be moved freely over the table. We acquired the data with intervals of movement and pause, and then run the optimisation algorithm. Next, we draw the error in a $3--D$ graph, where x and y correspond to the position and z to the error. See in figure H.2, top, that the error is lower (higher in the graphic) at certain intervals, those when the receiver had stopped its motion.

RL

Another experiment, this time following the geometry of a line, confirmed the previous results. To achieve this geometry, we attached a ruler to a table, and slipped the receiver along the ruler while acquiring the data. See in table H.2 that the accuracy is similar to that of the previous. Also, see in figure H.2, bottom, that the error presents some dependency on the position. The shape of the error function is regular despite the fact that several runs along the ruler were made.

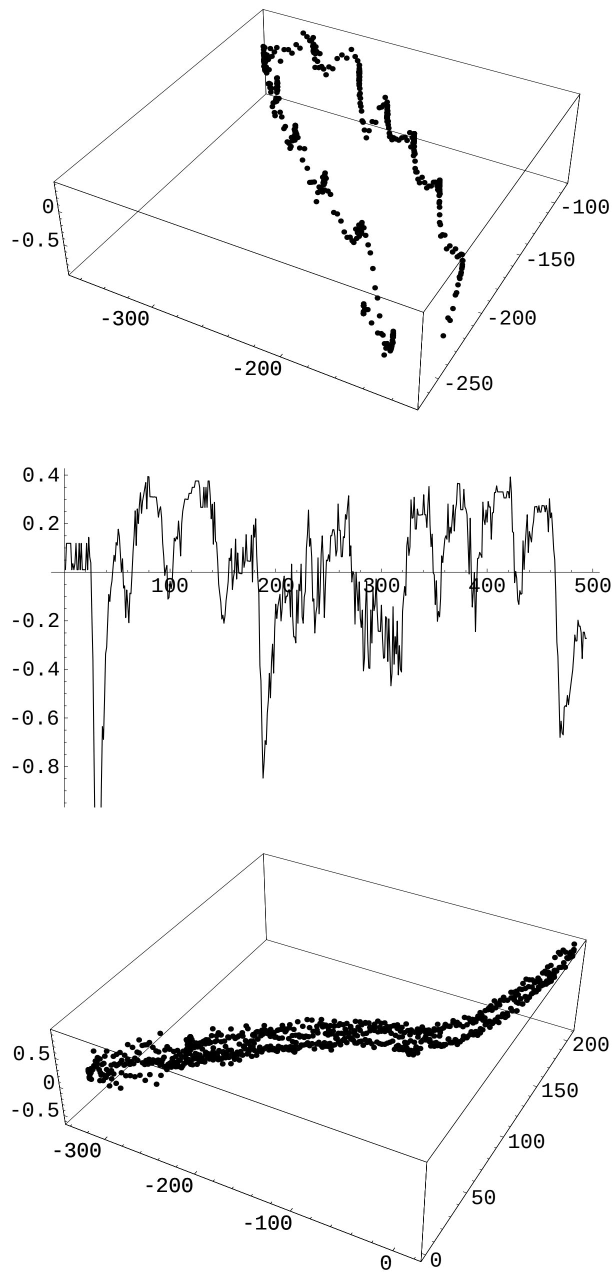

Figure H.2: RP3 Error as function of position in (x, y) (top) and varying in time (middle). **RL** Error as function of position in (x, y) (bottom)

S.	#	T_x (mm)	T_y (mm)	R_x (deg)	R_y (deg)	RMS (mm)	StdDev (mm)	C.N.
1	756	192.84	32.98	7.55	31.17	0.47	0.27	3.58

Table H.4: Numerical results of experiment **RL**.

H.3 SP, SL and SS

We attached the receiver to a stylus, and made a similar set of experiments. Now there is a larger set of values to optimise, and the experiment is close to those with the ecographer. The matrix M_U^R is not the identity matrix any longer. Also, now the orientation of the receiver is included in the equations, thus introducing a new source of errors.

Tables H.3, H.3 and H.3 report the numerical results for the models of plane, line and point. For all, the values of the solution are far more irregular the before, and the RMS error is much higher. The explanation is that the orientation output of the tracker is much more sensitive to noise, because of the shape of the object. In effect, the distance between the tip of the stylus to the receiver make small errors of orientation become higher. Also, there occur a number of glitches, which simply give wrong data values. While the optimisation algorithm is designed to be robust against these effects, if they are too numerous the final solution is not reproducible.

In order to see this effect, we have drawn the error in the y scale as function in time, for experiment **SP**. See in figure H.3 that the glitches occur in all datasets, but they are specially important in datasets 1 and 2, which are those presenting highest rms error in table H.3.

S.	#	M_U^R			M_T^C			RMS	StdDev	C.N.
		T_z (mm)	R_x (deg)	R_y	T_x (mm)	T_y	T_z	(mm)	(mm)	
1	357	122.66	0.39	0.5	2.93	1.22	8.64	3.15	4.43	39.55
2	350	95.52	0.12	1.77	30.6	-4.84	8.95	2.56	3.82	30.27
3	373	86.1	-0.29	1.24	40.55	2.41	9.04	0.62	0.94	45.5
4	385	97.75	-0.39	1.06	28.21	1.92	5.77	1.38	1.96	64.78
5	354	100.1	0.5	0.51	28.86	0.4	6.21	1.4	2.29	47.49
6	1819	98.64	-0.19	1.12	27.01	-0.2	8.93	1.99	3.32	31.9

Table H.5: Numerical results for experiment **SP**

H.4 Remarks

The experiments performed have been useful at giving some idea of the problems to expect to calibrate the ecographer. The most disturbing effect is the glitches in the orientation of the receiver, but also the effect of the movement to the accuracy of the

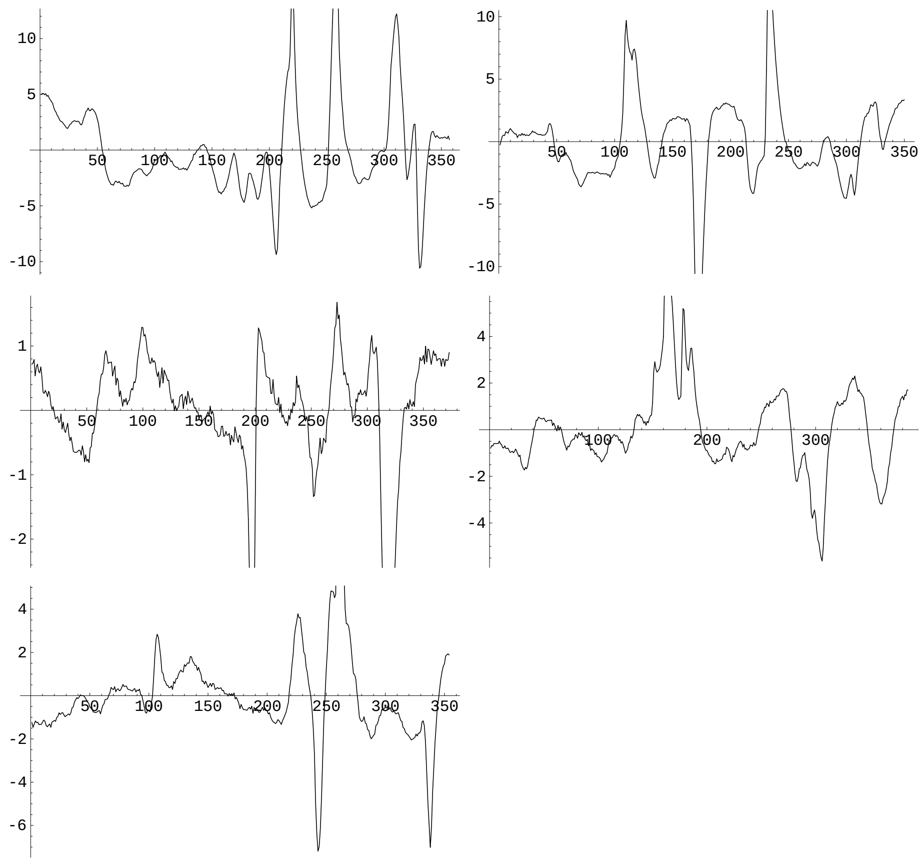

Figure H.3: SP Error as function of time for datasets 1 to 5. (Note the different scaling in y)

S.	#	M_U^R				M_T^C			RMS	StdDev	C.N.
		T_x	T_y	R_x	R_y	T_x	T_y	T_z			
		(mm)		(deg)		(mm)			(mm)	(mm)	
1	261	153.64	84.65	1.35	26.84	40.93	-0.73	8.6	2.19	1.25	55.17
2	257	153.25	84.16	1.68	26.84	40.89	1.88	9.	1.62	0.93	45.06
3	276	148.92	85.67	1.06	26.62	42.58	0.32	11.16	1.76	0.95	55.47
4	270	154.06	83.84	0.67	26.97	43.95	1.93	8.84	2.08	1.01	37.93
5	259	152.8	87.64	1.01	26.42	38.94	3.54	8.02	1.46	0.82	48.07
6	1323	153.81	84.19	1.43	26.91	41.58	1.5	8.64	1.85	1.2	29.41

Table H.6: Numerical results for experiment **SL**

S.	#	M_U^R			M_T^C			RMS	StdDev	C.N.
		T_x	T_y	T_z	T_x	T_y	T_z			
		(mm)			(mm)			(mm)	(mm)	
1	254	247.1	6.37	81.32	44.26	-2.15	5.74	5.98	2.3	17.32
2	261	245.61	7.85	62.33	60.77	-0.86	6.21	7.17	2.93	9.77
3	257	257.54	2.39	118.56	2.12	-7.28	7.98	11.94	5.27	11.1
4	310	246.69	5.31	78.4	46.45	0.47	8.69	5.85	3.23	21.58
5	269	247.88	5.22	78.25	45.84	2.07	10.82	5.53	2.48	20.9
6	1351	256.49	1.62	117.6	3.32	-2.1	9.44	11.87	6.4	6.29

Table H.7: Numerical results for experiment **SS**

sensor. These problems could be taken into account later, thus making simpler the design step.

Also, we found the experiments very useful in order to provide programming structures common to all geometric models. In the Mathematica software package, we programed the optimisation scheme as a separate module, so for each model we only needed to specify the equations in a standard format.

Bibliography

[1] A. Apicella, J.S. Kippenhan, and J.H. Nagel. Fast multi-modality image matching. *SPIE*, 1092:252–262, 1989.

[2] K.S. Arun, T.S. Huang, and S.D. Blostein. Least-sqaures fitting of two 3–d point sets. *IEEE Transactions on pattern analysis and machine intelligence*, 9(5):698–700, September 1987.

[3] R.H.S. Carpenter. *Movements of the eyes*. Pion, London, 2 edition, 1988.

[4] Qin-sheng Chen, Michel Defrise, and F. Deconinck. Symmetric phase-only matched filtering of fourier-mellin transforms for image registration and recognition. *PAMI*, 16(12):1156–1168, Dec 1994.

[5] A. Collignon, F. Maes, D. Delaere, D. Vandermeulen, P. Suetens, and G. Marchal. Automated multi-modality image registration based on information theory. In Y. Bizais, C. Barillot, and R. Di Paola, editors, *Information Processing in Medical Imaging*, pages 263–274. Kluwer Academic, Dordrecht. The Netherlands., 1995.

[6] Christos Davatzikos and R.N. Bryan. Using a deformable surface model to obtain ashape representation of the cortex. *TMI*, 15(6):785–795, Dec 1996.

[7] Koichiro Deguchi, Junko Noami, and Hidekata Hontani. 3d fundus pattern reconstruction and display from multiple fundus images. In *"Proceedings of the International Conference on Pattern Recognition"*, volume 4, pages 94–97, 2000.

[8] Northern digital. Technical specifications for optotrack `http://www.ndigital.com/optotrak.html`.

[9] J. Domingo, G. Ayala, A. Simó, E. de Ves, L. Martínez-Costa, and P. Marco. Irregular motion recovery in fluorescein angiograms. *Patter recognition letters*, 18:805–821, 1997.

[10] D. Eberly, R. Gardner, B. Morse, S. Pizer, and C. Scharlach. Ridges for image analysis. *Journal of Mathematical Imaging and Vision*, 4:353–373, 1994.

[11] PJ Edwards, A King, DLG Hill, and DJ Hawkes. Stereo augmented reality in the surgical microscope. In *Proc. Medicine Meets Virtual Reality'99*, 1999.

[12] A.E. Elsner, L. Moraes, E. Beausencourt, et al. Scanning laser reflectometry of retinal and subretinal tissues. *Optics express*, 6(13):243–250, 2000.

[13] Matthieu Ferrant, Simon K. Warfield, Arya Nabavi, Ferenc A. Jolesz, and Ron Kikinis. Registration of 3d intraoperative MR images of the brain using a finite element biomechanical model. In *MICCAI*, pages 19–28, 2000.

[14] J. Michael Fitzpatrick. The retrospective registration evaluation project. `http://www.vuse.vanderbilt.edu/~image/registration/reg_eval_html/lloret%_2.html`.

[15] J. Michael Fitzpatrick, Derek L. G. Hill, Yu Shyr, Jay West, Colin Sudholme, and Calvin R. Maurer. Visual assessment of the accuracy of retrospective registration of MR and CT images of the brain. *IEEE transaction on medical imaging*, 17(4):571–585, August 1998.

[16] J. Michael Fitzpatrick, Jay B. West, and Calvin R. Maurer. Prediction error in rigid-body point-based registration. *IEEE Transactions on medical imaging*, 17(5):694–702, October 1998.

[17] Y. Ge and M. Fitzpatrick. Intersubject brain image registration using both cortical and subcortical landmarks. volume 2434, pages 81–95. SPIE, 1995.

[18] Y. Ge, M. Fitzpatrick, J. Bao, et al. A new method for identifying cortical convolutions in mr brain images. volume 2167, pages 484–496. SPIE, 1994.

[19] A.H. Gee, R.W. Prager, and L. Berman. Non-planar reslicing for freehand 3-d ultrasound. In Springer, editor, *Proceedings of the 2nd International Conference on Medical Image Computing and Computer-Assisted Intervention*, volume LNCS 1679, pages 716–725, 1999.

[20] A.S. Glassner, editor. *Graphics gems*, chapter Digital cartography for computer graphics, pages 307–325. Academic Press.

[21] G. Golub and C. van Loan. *Matrix Computations*, chapter 7.3.1. The Johns Hopkins University Press.

[22] R. Gonzalez and P. Wintz. *Digital Image Processing*. Addison-Wesley, second edition, 1987.

[23] R.C. Gonzalez and P. Wintz. *Digital image processing*. Addison–Wesley, 1977.

[24] M.A. González Ballester, A. Zisserman, and M. Brady. Segmentation and measurement of brain structures in mri including confidence bounds. *Medical Image Analysis*, 4(189–200), 2000.

[25] Lisa Gottesfeld Brown. A survey of registration techniques. *ACM Computer Surveys*, 24(4):325–376, Dec 1992.

[26] George J. Grevera and Jayaram K. Udupa. An objective comparison of 3–d image interpolation methods. *TMI*, 17(4):642–652, Aug 1998.

[27] Jiang H., R.A. Robb, and K.S. Holton. A new approach to 3–d registration of multimodality medical images by surface matching. In *Visualization in biomedical computing*, pages 196–213. SPIE Press, Bellingham, WA, 1992.

[28] A. Hagemann, Karl Rohr, H. Siegfried Stiehl, U. Spetzger, and J. M. Gilsbach. A biomechanical model of the human head for elasitc registration of MR-images. In *Bildverarbeitung fur die Medizin*, pages 44–48, 1999.

[29] P.F. Hemler, T.S. Sumanaweera, and P.A. van den Elsen. A versatile system for multimodality image fusion. *J. Image Guided Surgery*, 1:35–45, 1995.

[30] D.L.G. Hill and D.J. Hawkes. *Proceedings SPIE*, volume 2359, chapter Voxel similarity measures for automated image registration, pages 205–216. SPIE, 1994.

[31] D.L.G Hill, D.J. Hawkes, N. Harrison, and C.F. Ruff. *Information processing in medical imaging 1993*, chapter A strategy for multimodality registration incorporating anatomical knowledge and image characteristics. Springer-Verlag, 1993.

[32] J.M. Hollerbach and C.W. Wampler. The calibration index and taxonomy for robotic kinematic calibration methods. *Intl. j. robotics research*, 14:573–591, 1996.

[33] J.M. Hollerbach and C.W. Wampler. The calibration index and the role of input noise in robot calibration. In *Robotics research: the seventh international symposium*, pages 558–568. Springer-Verlag, London, 1996.

[34] IBM. Pietà project. `http://www.research.ibm.com/pieta`.

[35] M. Ikits and J.M. Hollerbach. Kinematic calibration using a plane constraint. In *Proceedings IEEE International conference on robotics and automation*, pages 3191–3196, Apr 1997.

[36] J. Koenderink and A. van Doorn. Local features of smooth shapes: ridges and courses. In *Geometric Methods in Computer Vision II*, volume 2031, pages 2–13. SPIE, 1993.

[37] J. Koenderink and A. van Doorn. Two-plus-one-dimensional differential geometry. *Pattern Recognition Letters*, 15:439–443, 1994.

[38] J. J. Koenderink and A. J. van Doorn. Relief: pictorial and otherwise. *Image and Vision Computing*, 13:321–334, 1995.

[39] Charles L. Lawson and Richard J. Hanson. *Solving least squares problems.* Prentice-Hall, 1974.

[40] D. Lemoine, D. Liegeard, E. Lussot, and C. Barillot. *Medical imaging 1994: Image capture, formatting and display*, volume 2164, chapter Multimodal registration system for the fusion of MRI, CT, MEG and 3D or stereotactic angiographic data, pages 46–56. Proceedings SPIE, 1994.

[41] Feng Lin and Robert D. Brandt. Towards absolute invariants of images under translation, rotation and dilation. *Pattern recognition letters*, 14:369–379, May 1993.

[42] D. Lloret, A. López Peña, J. Serrat, and J.J. Villanueva. Creaseness-based CT and MR registration: comparison with the mutual information method. *Journal of Electronic Imaging*, 8(3):255–262, July 1999.

[43] David Lloret. Results of retinographies in mpeg format. `http://www.cvc.uab.es/~david/retina`.

[44] David Lloret, A.M. López Peña, and Joan Serrat. Rigid registration of CT and MR volumes based on rothe's creases. In A. Sanfeliu, J.J. Villanueva, and A. Vitrià, editors, *7h Spanish Symposium on Pattern Recognition and Image Analysis*, pages 1–6. Asociación Española de Reconocimiento de Formas y Análisis de Imágenes, 1997.

[45] David Lloret, Cástor Mariño, Joan Serrat, Antonio M. López, Manuel G. Penedo, F. Gómez Ulla, and Juan J. Villanueva. Automatic registration of full slo video sequences. *IEEE Transactions On Medical Imaging*, 2001 (submitted).

[46] David Lloret, Cástor Mariño, Joan Serrat, Antonio M. López, and Juan J. Villanueva. Landmark-based registration of full slo video sequences. In Salvador Sánchez and Filiberto Pla, editors, *9th Spanish Symposium on Pattern Recognition and Image Analysis*, pages 189–194. Asociación Española de Reconocimiento de Formas y Análisis de Imágenes, 2001.

[47] David Lloret and Joan Serrat. System for calibration of a stereotactic frame. In M.I. Torres and A. Sanfeliu, editors, *8th Spanish Symposium on Pattern Recognition and Image Analysis*, pages 25–26. Asociación Española de Reconocimiento de Formas y Análisis de Imágenes, 1999.

[48] David Lloret, Joan Serrat, Antonio M. López Peña, Andrés Soler, and Juan J. Villanueva. Retinal image registration using creases as anatomical landmarks. In *Proceedings of the International Conference on Pattern Recognition*, volume 3, pages 207–210. IEEE Computer Society, 2000.

[49] G. Lohmann and Y. von Cramon. Automatic labelling of the human cortical surface using sulcal basins. *Medical Image Analysis*, 4:179–188, 2000.

[50] Noemi Lois, A.S. Halfyard, C. Bunce, Alan C. Bird, and F.W. Fitzke. Reproducibility of fundus autofluorescence measurements obtained using a confocal scanning laser ophthalmoscope. *Br. J. Ophthalmoloscopy*, 83:276–279, March 1999.

[51] A. López Peña and J. Serrat. Tracing crease curves by solving a system of differential equations. In B. Buxton and R. Cipolla, editors, *4th Euro. Conf. on Computer Vision*, volume 1064 of *Lecture Notes in Computer Science*, pages 241–250. Springer-Verlag, 1996.

[52] A.M. López Peña, D. Lloret, and J. Serrat. Creaseness measures for CT and MR image registration. In *Proceedings of the Conference on Computer Vision and Pattern Recognition'98*, pages 694–699. IEEE Computer Society, 1998.

[53] A.M. López Peña, F. Lumbreras, and J. Serrat. Creaseness from level set extrinsic curvature. In *Computer Vision-ECCV'98*, volume 1407, pages 156–169. Springer, 1998.

[54] F. Maes, A. Collignon, D. Vandermeulen, G. Marchal, and P. Suetens. Multimodality image registration by maximization of mutual information. *IEEE Trans. on Medical Imaging*, 16(2):187–198, April 1997.

[55] G.Q. Maguire, M.E. Noz, H. Rusinek, J. Jaeger, et al. Graphics applied to medical image registration. In *IEEE Computer Graphics applied*, volume 11, pages 20–29, 91.

[56] J. Maintz, P. van den Elsen, and M. Viergever. Evaluation of ridge seeking operators for multimodality medical image matching. *IEEE Trans. on Pattern Analysis and Machine Intelligence*, 18(4):353–365, 1996.

[57] J. Maintz, P. van den Elsen, and M.A. Viergever. Comparison of feature-based matching of ct and mr brain images. In N. Ayache, editor, *Computer Vision, Virtual Reality and Robotics in Medicine*, volume 905 of *Lecture Notes in Computer Science*, pages 219–228. Springer-Verlag, 1995.

[58] J. Maintz, P. van den Elsen, and M.A. Viergever. Comparison of edge-based and ridge-based registration of CT and MR brain images. *Medical image analysis*, 1:151–161, 1996.

[59] J. Maintz and M. Viergever. A survey of medical image registration. *Medical Image Analysis*, 2(1):1–36, 1998.

[60] G. Malandain, S. Fernández-Vidal, and J.M. Rocchisiani. Improving registration of 3–d medical images using a mechanical based method. In *European conference on Computer Vision*, pages 131–136, 1994.

[61] G. Malandain, S. Fernández-Vidal, and J.M. Rocchisiani. Rigid registration of 3–d objects by motions analysis. In *Proceedings 12th International Conference on Pattern Recognition*, pages 579–581, 1994.

[62] G. Malandain, S. Fernández-Vidal, and J.M. Rocchisiani. Physically based rigid registration of 3–d free-form objects: application to medical imaging. Technical Report 2453, INRIA, 1995.

[63] P. Marais and J.M. Brady. Detecting the brain surface in sparse mri using boundary models. *Medical Image Analysis*, 4:283–302, 2000.

[64] C Mariño, V.M. Gulías, M.G. Penas M., Penedo, V. Leborán, A. Mosquera, M.J. Carreira, and D. Lloret. Sistema de interpretación automática de secuencias slo basado en un servidor vod. In *Proceedings of the SIT2001*, 2001.

[65] L. Martínez-Costa, P. Marco, G. Ayala, E. de Ves, J. Domingo, and A. Simó. Macular edema computer-aided evaluation in ocular vein occlusions. *Computers and biomedical research*, 31:374–384, 1998.

[66] M. Elena Martínez-Pérez, Alun D. Hughes, ALice V. Stanton, and Simon A. Thom. Retinal blood vessel segmentation by means of scale-space analysis and region growing. In Chris Taylor and Alan Colchester, editors, *Medical image computing and computer-assisted intervention-MICCAI'99*, volume 1679 of *Lecture notes in computer science*, pages 90–97. Springer, 1999.

[67] B.R. Masters. Three-dimensional confocal microscopy of the human optic nerve in vivo. *Optics express*, 3(10):356–359, Nov 1998.

[68] Calvin R Maurer, Derek L.G. Hill, Alastair J. Martin, Haiying Liu, Michael McCue, Daniel Rueckert, David Lloret, Walter A. Hall, Robert E. Maxwell, David J. Hawkes, and Charles L. Truwit. Measurement of intraoperative brain deformation using a 1.5 tesla interventional MR system: Preliminary results. *IEEE Transactions on medical imaging*, 17(5):817–825, October 1998.

[69] W. Niblack. *An Introduction to Digital Image Processing*. Prentice-Hall, 1986.

[70] J. Noack and D. Sutton. An algorithm for the fast registration of image sequences obtained with a scanning laser opththalmoscope. *Phys. Med. Bio.*, 39:907–915, 1994.

[71] C.A. Pelizzari, G.T.Y. Chen, and T.R. Spelbring. Accurate 3-d registration of ct, pet and/or mr images of the brain. *J. Computed Assisted Tomography*, 13:20–26, 1989.

[72] A.M. López Peña. *Multilocal methods for ridge and valley delineation in image analysis*. PhD thesis, Universitat Autònoma de Barcelona, 1999.

[73] Graeme P. Penney, Jürgen Weese, Paul Desmedt, Derek L.G. Hill, and David Hawkes. A comparison of similarity measure for use in 2-d–3-d medical image registration. *TMI*, 17(4):586–595, Aug 1998.

[74] Arya Nabavi Peter. Serial intraoperative mr imaging of brain shift.

[75] Axel Pinz, Stefan Bernogger, Peter Datlinger, and Andreas Kruger. Mapping the human retina. *IEEE Transactions on Medical Imaging*, 17(4):606–619, Aug 1998.

[76] Axel Pinz, Manfred Prantl, and Harald Ganster. Affine matching of intermediate symbolic representations. In V. Hlavác, editor, *Proceedings of Computer Analysis of Images and Patters CAIP'95*, volume 970, pages 359–367, 1995.

[77] Axel Pinz, Manfred Prantl, and Harald Ganster. A robust affine matching algorithm using an exponentially decreasing distance function. *Journal of Universal Computer Science*, 1(8):614–631, 1995.

[78] R.W. Prager, A.H. Gee, and L. Berman. Stradx: real–time acquisition and visualisation of freehand 3d ultrasound. Technical Report 319, Dept. of Engineering, Univ. of Cambridge, Apr 1998.

[79] R.W Prager, R.N. Rohling, A.H. Gee, and L. Berman. Automatic calibration for 3–d free-hand ultrasound. Technical Report CUED/F-INFENG/TR 303, Cambridge university engineering department, Sep 1997.

[80] W. Press, S. Teukolsky, W. Vetterling, and B. Flannery. *Numerical Recipes in C.* Cambridge University Press, 2 edition, 1992.

[81] Nicola Ritter, Robyn Owens, and James Cooper. Registration of stereo and temporal images of the retina. *IEEE Transactions on Medical Imaging*, 18(5):404–418, May 1999.

[82] D. Roberts, A. Hartov, F. Kennedy, M. Miga, and K. Paulsen. Intraoperative brain shift and deformation: A quantitative analysis of cortical displacement in 28 cases. *Neurosurgery*, 43(4):749–760, 1998.

[83] N.R. Rohling. 3–d ultrasound imaging: optimal volumetric reconstruction. Technical report, Dept. of Engineering, Univ. of Cambridge, May 1996.

[84] N.R. Rohling and A.H. Gee. Issues in 3–d free–hand medical ultrasound imaging. Technical Report CUED/F-INFENG/TR 246, Cambridge University Department of Engineering, Jan 1996.

[85] R. Rohling, A. Gee, and L. Berman. Three-dimensional spatial compounding of ultrasoud images. *Medical Image Analysis*, 1(3):177–193, 1996–97.

[86] R.N. Rohling. *3D freehand ultrasound: reconstruction and spatial compounding.* PhD thesis, University of Cambridge, 1998.

[87] R.N. Rohling, A.H. Gee, and L. Berman. Radial basis function interpolation for 3–d ultrasound. Technical Report CUED/F-INFENG/TR 327, Cambridge university engineering department, Jul 1998.

[88] Robert Rohling and Andrew Gee. Correcting motion-induced registration errors in 3-d ultrasound images. In *Proceedings of the British Machine Vision Conference*, volume 2, pages 645–654, 1996.

[89] Royce Sadler. *Numerical methods for nonlinear regression.* University of Queensland press, 1975.

[90] M.R. Spiegel and L. Abellanas. *Fórmulas y tablas de matemática aplicada.* McGraw Hill, 1994.

[91] B. Srinivasa Reddy and B. N. Chatterji. An fft-based technique for translation, rotation and scale-invariant image registration. *TIP*, 5(8):1266–1271, Aug 1996.

[92] C. Studholme, D. Hill, and D. Hawkes. Multiresolution voxel similarity measures for MR-PET registration. In *Information Processing in Medical Imaging*, 1995.

[93] C. Studholme, D.L.G. Hill, and D.J. Hawkes. Automated 3d registration of mr and ct images of the head. *Medical image analysis*, 1996.

[94] C. Studholme, D.L.G. Hill, and D.J. Hawkes. Automated three-dimensional registration of MR and PET brain images by multiresolution optimization of voxel similarity measure. *Medical physics*, 24(1):25–35, January 1997.

[95] M. Syn and R. Prager. Mesh models for three-dimensional ultrasound imaging, 1994.

[96] Michael Hsien-Min Syn. Model-based three-dimensional freehand ultrasound imaging.

[97] Transtech systems. Technical specifications for videoport framegrabber `http://www.transtech-systems.co.uk/framegrabbers/vppro1.htm`.

[98] Ascencion technology corporation. Technical specifications for minibird 800 `http://www.ascension-tech.com/products/minibird/details.html#Specificat%ions`.

[99] Yannis A. Tolias and Stavros M. Panas. A fuzzy vessel tracking algorithm for retinal images based on funzzy clustering. *IEEE Transactions on Medical Imaging*, 17(2):263–273, April 1998.

[100] Graham Treece, Richard Prager, Andrew Gee, and Laurence Berman. 3d ultrasound measurement of large organ volume. *Medical Image Analysis*, 5:41–54, 2001.

[101] P. Tuomola, A. Gee, R. Prager, and L. Berman. Body-centered visualisation for freehand 3d ultrasound, 2000.

[102] P. van den Elsen, J. Maintz, E-J. Pol, and M. Viergever. Automatic registration of CT and MR brain images using correlation of geometrical features. *IEEE Trans. on Medical Imaging*, 14(2):384–396, 1995.

[103] P. van den Elsen, E-J. Pol, T. Sumanaweera, P. Hemler, S. Napel, and J. Adler. Grey value correlation techniques used for automatic matching of CT and MR brain and spine images. In *Visualization in Biomedical Computing*, volume 2359, pages 227–237. SPIE, 1994.

[104] P. van den Elsen, E.J.D. Pol, and M.A. Viergever. Medical image matching– a review with classification. *IEEE Engn Med. Biol.*, 12:26–39, 1993.

[105] Pedro Vieira, A. Manivannan, C.S. Lim, and J.V. Forrester. Tomographic reconstruction of the retina using the confocal scanning laser ophthalmoscope. *Physiological measurement*, 20:1–19, 1999. `http://www.biomed.abdn.ac.uk/Abstracts/A03F00/`.

[106] A.R. Wade and F.W. Fitzke. A fast, robust pattern recognition system for low light level image registration and its application to retinal imaging. *Optics express*, 3(5):190–197, Aug 1998.

[107] M.Y. Wang, C.R. Maurer, J.M. Fitzpatrick, and R.J. Maciunas. An automatic technique for finding and localizing externally attached markers in ct and mr volume images of the head. *IEEE Transactions on Biomedical Eng.*, 43:627–637, 1996.

[108] Simon K. Warfield, Matthieu Ferrant, Xavier Gallez, Arya Nabavi, Ferenc A. Jolesz, and Ron Kikinis. Real-Time Biomechanical Simulation of Volumetric Brain Deformation for Image Guided Neurosurgery. In *SC 2000: High Performance Networking and Computing Conference; 20 00 Nov 4–10; Dallas, USA*, pages 230:1–16, 2000.

[109] Simon K. Warfield, Arya Nabavi, Torsten Butz, Kemal Tuncali, Stuart G. Silverman, Peter Black, Ferenc A. Jolesz, and Ron Kikinis. Intraoperative segmentation and nonrigid registration for image guided therapy. In *MICCAI*, pages 176–185, 2000.

[110] Robert H. Webb, Geoerge W. Hughes, and Francois C. Delori. Confocal scanning laser opthalmoscope. *Applied Optics*, 26(8), 1987.

[111] Robert H. Webb and George W. Hughes. Scanning laser opthalmoscope. *IEEE Transactions on Biomedical Engineering*, BME-28(7), July 1981.

[112] W. Wells, P. Viola, H. Atsumi, S. Nakajima, and R. Kikinis. Multi-modal volume registration by maximization of mutual information. *Medical Image Analysis*, 1(1):35–51, 1996.

[113] J. West, J. Fitzpatrick, M. Wang, B. Dawant, C. Maurer, R. Kessler, and R. Maciunas. Retrospective intermodality registration techniques: surface-based versus volume-based. In *Proceedings of CVRMED-MRCAS*, pages 151–160, 97.

[114] J. West, J. Fitzpatrick, M. Wang, B. Dawant, C. Maurer, R. Kessler, R. Maciunas, C. Barillot, D. Lemoine, A. Collignon, F. Maes, P. Suetens, D. Vandermeulen, P. van den Elsen, S. Napel, T. Sumanaweera, B. Harkness, P. Hemler, D. Hill, D. Hawkes, C. Studholme, J. Maintz, M. Viergever, G. Malandain, X. Pennec, M. Noz, G. Maguire, M. Pollack, C. Pelizzari, R. Robb, D. Hanson, and R. Woods. Comparison and evaluation of retrospective intermodality brain image registration techniques. *J. Computational Assisted Tomography*, 21:554–556, 1997.

[115] S. Wolf, F. Jung, H. Kiesewetter, N Körber, and M. Reim. Video fluorescein angiography:methor and clinical application. *Graefe's Arch Clin Exp Ophthalmol*, 227:145–151, 1989.

[116] Inc Wolfram Research. Mathematica website `http://www.wolfram.com`.

[117] R.P. Woods, J.C. Mazziotta, and S.R. Cherry. MRI PET registration with automated algorithm. *Journal of computed assisted tomography*, 17:536–546, 1993.

[118] F. Zana and J.C. Klein. A multimodal registration algorithm of eye fundus images using vessels detection and hough transform. *IEEE transactions on Medical Imaging*, 18(5):419–428, May 1999.

Selected bibliography

- David Lloret, Joan Serrat, Antonio M. López, and Juan J. Villanueva. Ultrasound to mr volume registration for brain sinking measurement. *IEEE Transactions On Systems, Man and Cybernetics*, 2001 (submitted).

- David Lloret, Cástor Mariño, Joan Serrat, Antonio M. López, Manuel G. Penedo, F. Gómez Ulla, and Juan J. Villanueva. Automatic registration of full slo video sequences. *IEEE Transactions On Medical Imaging*, 2001 (submitted).

- D. Lloret, A. López, J. Serrat, and J.J. Villanueva. Creaseness-based CT and MR registration: comparison with the mutual information method. *Journal of Electronic Imaging*, 8(3):255–262, July 1999.

- A. López, D. Lloret, J. Serrat, and J.J. Villanueva. Multilocal creasness based on the level set extrinsic curvature. *Computer Vision and Image Understanding*, (77), 2000.

- Calvin R Maurer, Derek L.G. Hill, Alastair J. Martin, Haiying Liu, Michael McCue, Daniel Rueckert, David Lloret, Walter A. Hall, Robert E. Maxwell, David J. Hawkes, and Charles L. Truwit. Measurement of intraoperative brain deformation using a 1.5 tesla interventional MR system: Preliminary results. *IEEE Transactions on medical imaging*, 17(5):817–825, October 1998.

- David Lloret, Joan Serrat, Antonio M. López, Andrés Soler, and Juan J. Villanueva. Retinal image registration using creases as anatomical landmarks. In *Proceedings of the International Conference on Pattern Recognition*. IEEE Computer Society, 2000.

- David Lloret, Antonio López, and Joan Serrat. Precise registration of CT and MR volumes based on a new creaseness measure. In Stephen Marshall, Neal Harvey, and Druti Shah, editors, *Noblesse workshop on non-linear model based image analysis*, pages 15–20, 98.

- C Mariño, V.M. Gulías, M.G. Penas M., Penedo, V. Leborán, A. Mosquera, M.J. Carreira, and D. Lloret. Sistema de interpretación automática de secuencias slo basado en un servidor vod. In *Proceedings of the SIT2001*, 2001.

- David Lloret and Derek L.G. Hill. System for live fusion of 2–d ultrasound scans to pre-interventional mr volumes of a patient. In M.I. Torres and A. Sanfeliu, editors, *8th Spanish Symposium on Pattern Recognition and Image Analysis*, pages 23–24. Asociación Española de Reconocimiento de Formas y Análisis de Imágenes, 1999.

- David Lloret, A.M. López, and Joan Serrat. Rigid registration of CT and MR volumes based on rothe's creases. In A. Sanfeliu, J.J. Villanueva, and A. Vitrià, editors, *7h Spanish Symposium on Pattern Recognition and Image Analysis*, pages 1–6. Asociación Española de Reconocimiento de Formas y Análisis de Imágenes, 1997.
- David Lloret and Joan Serrat. System for calibration of a stereotactic frame. In M.I. Torres and A. Sanfeliu, editors, *8th Spanish Symposium on Pattern Recognition and Image Analysis*, pages 25–26. Asociación Española de Reconocimiento de Formas y Análisis de Imágenes, 1999.
- A.M. López, D. Lloret, and J. Serrat. Creaseness measures for CT and MR image registration. In *Proceedings of the Conference on Computer Vision and Pattern Recognition'98*, pages 694–699. IEEE Computer Society, 1998.